# Convective invigoration traced to warm-rain microphysics

Xin Rong Chua[1,1] and Yi Ming[2,2]

[1]Centre for Climate Research Singapore
[2]Geophysical Fluid Dynamics Laboratory

November 30, 2022

**Abstract**

Aerosols are postulated to alter moist convection by increasing cloud droplet number concentration. Cloud-resolving model simulations of radiative-convective equilibrium show that increased cloud droplet number concentration leads to higher convective mass flux, seemingly in line with a popular hypothesis which links the convective invigoration to delayed rain formation allowing more cloud liquid water to be frozen. Yet, the same phenomenon is also present in an alternative model configuration with only warm-rain microphysics, suggesting that one does not have to invoke ice microphysics. The key mechanism lies in the different vertical distributions of the increases in cloud liquid re-evaporation and in water vapor condensation, causing a dipole pattern that favors convection. This is further supported by a mechanism-denial experiment in which weakened cloud re-evaporation tends to mute invigoration. This work represents a major advancement of the process-level understanding of aerosol effects on convection.

# Convective invigoration traced to warm-rain microphysics

**Xin Rong Chua[1]\*, Yi Ming[1,2]**

[1]Program in Atmospheric and Oceanic Sciences, Princeton University, Princeton, New Jersey, USA

[2]Geophysical Fluid Dynamics Laboratory/NOAA, Princeton, New Jersey, USA

**Key Points:**

- Higher cloud droplet number concentration increases convective mass flux, even in the absence of ice microphysics.
- The convective invigoration coincides with higher tropospheric relative humidity and re-evaporation efficiency.
- The dynamical mechanism involves a vertical dipole (cooling-above-warming) pattern.

---

\*Current affiliation: Centre for Climate Research Singapore, Singapore

Corresponding author: Yi Ming, `Yi.Ming@noaa.gov`

**Abstract**

Aerosols are postulated to alter moist convection by increasing cloud droplet number concentration ($N_d$). Cloud-resolving model simulations of radiative-convective equilibrium show that higher $N_d$ leads to stronger convective mass flux, seemingly in line with a hypothesis that links the convective invigoration to delayed rain formation allowing more cloud liquid condensate to be frozen. Yet, the invigoration is also present in an alternative model configuration with warm-rain microphysics only, suggesting that ice microphysics is not central to the phenomenon. The key dynamical mechanism lies in the different vertical distributions of the increases in water vapor condensation and in cloud liquid re-evaporation, causing a dipole pattern favoring convection. This is further supported by a pair of mechanism-denial experiments in which an imposed weakening of cloud liquid re-evaporation tends to mute invigoration.

**Plain Language Summary**

Aerosols are thought to affect moist convection by increasing cloud droplet number concentration. According to a popular hypothesis, higher droplet number concentration would delay rain formation, allowing more cloud water to reach the freezing level. The additional latent heating from freezing is presumed to cause stronger convection. We test this hypothesis with a numerical model capable of simulating moist convection, and find that convective invigoration occurs even in the absence of ice processes. A detailed analysis suggests that the slowdown of rain formation increases cloud liquid re-evaporation. The resulting cooling is balanced primarily by stronger water vapor condensation. This creates a vertical cooling-above-warming dipole pattern favorable to convection.

## 1 Introduction

Aerosols, natural and anthropogenic alike, alter Earth's radiative budget by scattering and/or absorbing shortwave radiation, as well as by altering cloud albedo (Twomey, 1974) and lifetime (Albrecht, 1989). Both effects have important implications for moist convection and precipitation. This work focuses on the purely microphysical pathway through which aerosols affect deep convective clouds by increasing cloud droplet number concentration ($N_d$). A commonly referenced mechanism (Rosenfeld et al., 2008; Williams

et al., 2002; Andreae et al., 2004) posits that higher $N_d$ leads to smaller droplets, thus delaying rain formation. This effect tends to bring more cloud liquid water above the freezing level, and the additional latent heat release would invigorate convection.

Stevens and Feingold (2009) hypothesized that delayed precipitation formation would allow more liquid to reach the cloud-top region of a cumulus. The resulting re-evaporative cooling has an effect of destabilizing the atmospheric column, and thus promoting convection. It was also acknowledged that this cloud-dynamical effect might be mitigated by more efficient precipitation production in deep clouds. More broadly, the re-evaporation of cloud condensate, by influencing cold pool strength, can exert a strong control on subsequent convection (e.g. Tao et al., 2007; Morrison, 2012; Tao et al., 2012). A recent study by Fan et al. (2018) suggested that ultrafine aerosol particles (smaller than 50 nm) can be activated into cloud droplets in a clean environment owing to higher in-cloud supersaturation; the additional droplets in return facilitate condensation. It was argued that the resulting convective invigoration occurs via a warm-phase (liquid) microphysical pathway based on the relatively small increase in upper-level latent heating. In other words, one does not have to rely on ice microphysics to explain the convective adjustment to aerosols.

To further complicate the matter, there is no consensus among the existing case studies on how aerosols would strengthen or weaken convection (see Morrison (2012) for a case of weakening). It is not straightforward to make comparison across different case studies given that environmental factors such as wind shear (e.g. Fan et al., 2009) and cloud-radiative effects (e.g. Fan et al., 2015) can potentially alter the eventual convective response. In contrast, the setting of radiative-convective equilibrium (RCE) makes it possible to diagnose which processes are of leading-order importance to the simulated quasi-steady state in a simple framework. For example, van den Heever et al. (2011) found an increase in the frequency of updrafts in response to increased $N_d$. In a follow-up study focusing on deep convective clouds, Storer and van den Heever (2013) showed that the freezing of cloud liquid is not among the largest contributors to the overall latent heat budget, suggesting that at least in RCE, freezing might not be as important for understanding convective invigoration as initially thought. This study is conceived as a targeted mechanistic study of the role of liquid microphysics in determining aerosol effects on convection.

## 2 Methodology

The RCE simulations are performed with the Weather Research and Forecasting (WRF) model (Wang & Sobel, 2011), a widely used cloud-resolving model (CRM). The configuration is identical to that used in Chua et al. (2019) except for the treatment of cloud microphysics (as detailed later). The model domain is doubly periodic and contains 96×96 gridpoints at a horizontal resolution of 2 km with fifty vertical levels. Atmospheric radiative cooling is prescribed at -1.5 K day$^{-1}$ in the troposphere (defined as temperature warmer than 207.5 K). Elsewhere temperature is relaxed to 200 K over 5 days following a Newtonian relaxation scheme. Prescribing radiative cooling eliminates a major confounding factor common to this type of studies. Surface sensible and latent heat fluxes are computed with an aerodynamic formulation at a constant near-surface wind speed of 5 m s$^{-1}$. The surface temperature is set at 301 K. Subgrid diffusion is calculated with the Smagorinsky and YSU schemes (Hong et al., 2006). Domain-average winds are nudged to zero on a time scale of two hours.

The model uses the the double-moment Morrison cloud microphysics scheme (Morrison et al., 2009). By tracking both mass mixing ratios and numbers of hydrometeors, a double-moment scheme is deemed to be more suitable for simulating the microphysical effects of aerosols on moist convection than a single-moment scheme of mixing ratios. The warm-rain or liquid part of the scheme is described briefly here as it is important for understanding the results. Water vapor ($q_v$) condenses into cloud liquid ($q_l$) through saturation adjustment. Note that $q$ denotes mass mixing ratio. Re-evaporation of cloud liquid occurs only under subsaturated conditions. Cloud liquid converts into rain ($q_r$) through either autoconversion or accretion; the rates are parameterized as $1350q_l^{2.47}N_d^{-1.79}$ and $67(q_lq_r)^{1.15}$, respectively (Khairoutdinov & Kogan, 2000). Note that $q_l$ and $q_r$ are in kg kg$^{-1}$, $N_d$ in cm$^{-3}$ and the rates in kg kg$^{-1}$ s$^{-1}$. Autoconversion is the only microphysical process that is controlled directly by $N_d$. Rain can re-evaporate back into water vapor.

Three alternative configurations are created from simplifying the full model (referred to as FU). One can turn off the ice part of the Morrison scheme. In the resulting configuration (referred to as LI), the liquid microphysics operates at all temperatures. The formulae used for computing the cloud liquid and rain re-evaporation rates are scaled

106    by a factor of 0.1 in the CE and RE configurations, respectively. This does not mean that

107    the actual rates would decrease by 10 times as other factors may also vary.

108      For each of the four model configurations (i.e. FU, LI, CE and RE), a pair of sim-

109    ulations are performed. $N_d$ is set to 100 cm$^{-3}$ in the control experiment, and 1000 cm$^{-3}$

110    in the perturbation experiment. The former is denoted by the name of a configuration,

111    and the latter by adding an asterisk. For example, the control and perturbation exper-

112    iments performed with the full model are referred to as FU and FU*, respectively.

113      A control experiment is initialized from a warm bubble, and is integrated for 240

114    model days. The output at Day 180 is used to initialize a corresponding 60-day pertur-

115    bation experiment. We analyze the last 20 days of hourly-mean outputs from each sim-

116    ulation. The noise level of a given variable is quantified using five consecutive, non-overlapping

117    20-day periods from an extended full model control simulation (namely FU).

## 3   Results

119      Some key characteristics of the control simulations and their changes in response

120    to higher $N_d$ are depicted in Figure 1. The distributions of cloud liquid ($q_l$) in the lower

121    and mid-troposphere are similar among all four configurations, with a distinct peak at

122    around 900 hPa (Figure 1a). As designed, high clouds are comprised of ice ($q_i$) in FU,

123    and liquid in the other cases. Interestingly, the upper-tropospheric $q_l$ in LI and CE is

124    comparable to $q_i$ in FU, but much higher than $q_l$ in RE. Higher $N_d$ gives rise to an in-

125    crease in cloud condensate below 500 hPa in all cases (Figure 1b). CE is opposite to the

126    other three cases in showing a substantial increase in high cloud condensate.

127      In FU, rain ($q_r$) is concentrated mostly below 500 hPa, while snow and graupel (col-

128    lectively referred to as snow, $q_s$) dominates above. The three liquid microphysics con-

129    trol simulations exhibit almost identical vertical distributions of rain throughout the col-

130    umn, which are bottom-heavy with maxima at around 700 hPa (Figure 1c). Elevated

131    $N_d$ causes $q_r$ to decrease in all cases below 600 hPa, and to increase in the three liquid

132    microphysics cases above, albeit to varying degrees (Figure 1d). $q_s$ in FU increases as

133    well. Taken together, the increase in cloud liquid and the concurrent decrease in rain in

134    the lower troposphere are consistent with the microphysical nature of the perturbation,

135    i.e. higher $N_d$ tending to suppress the conversion of cloud liquid to rain, while convec-

136    tive adjustment seems to play a prominent role in shaping the upper-tropospheric changes.

Convective mass flux ($M_c$) is computed by summing the mass flux at gridpoints where the total cloud condensate ($q_c$, or $q_l + q_i$) is greater than 0.005 g kg$^{-1}$ and vertical velocity exceeds 1 m s$^{-1}$ (Wang & Sobel, 2011). In much of the troposphere, $M_c$ in FU is substantially (about 40%) stronger than in the liquid microphysics cases (Figure 1e). They also differ in vertical structures; FU has only one in the lower troposphere, while the latter have two peaks, one in the lower troposphere and the other in the upper troposphere. $M_c$ shows a substantial increase below 500 hPa due to higher $N_d$, which amounts to ∼30% at 600 hPa (Figure 1f). The convective invigoration is accompanied by a relatively small decrease in $M_c$ in the upper troposphere in FU* and LI*. The magnitude of the enhancement of $M_c$ is fully captured in LI, suggesting that ice microphysics is not essential for explaining the convective invigoration, contrary to Rosenfeld et al. (2008). Furthermore, the invigoration is muted in the configuration of CE, indicating that cloud liquid re-evaporation may be a key process involved in the convective response. In contrast, RE does not show any appreciable difference from LI, which hints at a secondary role played by rain re-evaporation. Note that none of the simulations examined here shows any sign of self-aggregation.

Figure 1g shows the relative humidity ($RH$) in the control cases. The vertical profiles take a C-shape, with minima at around 500 hPa. FU, however, has notably higher mid-tropospheric $RH$ (∼70%) than the liquid microphysics cases (∼40%), suggesting that ice microphysics is crucial for moistening the mid-troposphere. A comparison of RE and LI indicates that rain re-evaporation is also an important source of mid-tropospheric moisture, while cloud liquid re-evaporation is not (CE versus LI). Across all cases, $RH$ shows a pronounced increase below 500 hPa owing to higher $N_d$ (Figure 1h). With the exception of CE, they all experience lower $RH$ in the upper troposphere.

The impression from Figures 1(f) and (h) that convective invigoration coincides with mid-tropospheric moistening is formalized in Figure 2. The vertically averaged convective mass flux ($[M_c]$) in the various control and perturbation experiments is generally positively correlated with the column-average relative humidity ($CRH$). The correlation with the mid-tropospheric (400 to 600 hPa) relative humidity ($MRH$) is even stronger. This relationship holds not only for every pair of control and perturbation experiments but also for all the control experiments. Although it is well established that a moist mid-troposphere is conducive to convective development (e.g. in the context of tropical cyclones), convective detrainment of cloud condensate is an important supplier

170  of mid-tropospheric moisture. These two mechanisms are not mutually exclusive, and

171  work in the same direction. This work does not attempt to address the relative roles of

172  these mechanisms, which would be difficult to separate in a clean way.

173  The need to better understand the controlling factors of $RH$ prompts us to exam-

174  ine the moisture budget. The column-integrated source and sink terms, along with the

175  changes caused by increased $N_d$, are given in Table 1. To facilitate the discussion, they

176  are also illustrated in Figure 3 for the LI configuration. For water vapor, condensation

177  ($C$) is balanced by surface evaporation ($ES$), and re-evaporation of cloud condensate and

178  rain ($EC$ and $ER$, respectively). The conversion from cloud liquid to rain is realized through

179  autoconversion ($CR$) and accretion ($AR$). Although autoconversion is almost negligi-

180  ble in terms of domain average (consistent with other cloud-resolving simulations (e.g.

181  Heikenfeld et al., 2019)), it is the only process through which rain formation can occur

182  spontaneously – a necessary condition for accretion that involves both cloud liquid and

183  rain simultaneously. In this sense, it is conceivable that a perturbation to the former,

184  however small in magnitude, may still affect the latter. Rain is partitioned between re-

185  evaporation ($ER$) and surface precipitation ($P$).

186  The re-evaporation efficiency ($\alpha$) is defined as the ratio of the total re-evaporation

187  ($E$, or the sum of $EC$ and $ER$) to $C$ (Romps, 2014). Note that one definition of the widely

188  used quantity called precipitation efficiency is the ratio of surface precipitation ($P$) to

189  $C$ (e.g. Langhans et al., 2015; Lutsko & Cronin, 2018). Thus, $\alpha$ is one minus the pre-

190  cipitation efficiency. Dictated, to the zeroth order, by the free-tropospheric radiative cool-

191  ing rate, the domain-average $ES$ or $P$ is little changed regardless of the configurations

192  or perturbations. Both $C$ and $E$ are substantially lower in LI than in FU, but the frac-

193  tional decrease in $E$ is greater than that in $C$. This results in a net decrease in $\alpha$. As

194  expected, weakening the re-evaporation processes tends to lower $\alpha$, albeit to different ex-

195  tents. $\alpha$ is more sensitive to the perturbation to rain re-evaporation than that to cloud

196  liquid re-evaporation, implying that $EC$ is limited more strongly by the availability of

197  cloud liquid as opposed to the prescribed rate constant.

198  Higher $N_d$ leads to a slowdown in accretion by modulating autoconversion. This

199  is consistent with higher $q_l$ and lower $q_r$ (Figures 1b and d). As explained before, since

200  $P$ is somewhat fixed, and $\delta CR$ is small, $\delta AR$ must be approximately equal to $\delta ER$ (with

201  $\delta$ denoting changes). This explains why rain re-evaporation decreases. Higher $q_l$ is con-

sistent with stronger $EC$ as they are directly linked. Since $P$ is approximately unchanged, it follows that $\delta C \simeq \delta ER + \delta EC$. This relation, however, does not help constrain the sign of $\delta C$ as $\delta ER$ and $\delta EC$ are of opposite signs. It seems plausible to assume that $C$ and $EC$ would vary in the same direction as they are the dominant sink and source terms in the cloud liquid budget, an issue to which we will return later.

Invoking $\delta C \simeq \delta E$, one can write $\delta\alpha$ approximately as $(1-\alpha)\delta C/(C+\delta C)$. If it is assumed that $\delta C \ll C$, the expression can be further simplified to $\delta\alpha \simeq (1-\alpha)\delta C/C$. This simple theory is found to be in good agreement with the simulated $\delta\alpha$ (Table 1). Thus, the increase in $\alpha$ can be thought of as a manifestation of stronger condensation.

Across all the cases, $\alpha$ is strongly correlated with column relative humidity ($CRH$) (Figure 2c), and to a lesser extent, with mid-tropospheric relative humidity ($MRH$) (Figure 2d). This result is qualitatively consistent with an analytical model of tropospheric relative humidity in RCE (Romps, 2014), in which cloud condensate re-evaporation is treated as an important mechanism for moistening the environment. In particular, $\alpha$ is smaller than $CRH$, conforming to the constraint inferred from the analytical model. This line of reasoning appears to suggest that the microphysical perturbation caused by higher $N_d$ tends to increase the re-evaporation efficiency. The resulting tropospheric moistening creates a favorable environment for convection.

As appealing as the above explanation is, it does not yield insights into the dynamics underlying the convective invigoration. The microphysical processes discussed above can be divided into two categories depending on whether phase change is involved. The latent heating from condensation ($C$) and the latent cooling from rain and cloud condensation re-evaporation ($ER$ and $EC$, respectively) play crucial roles in the energy balance, and have to be in equilibrium with other diabatic (e.g. radiative) and dynamical terms (resolved and implicit). In contrast, accretion is not part of the energy balance. Furthermore, the latent heating and cooling have distinct vertical structures as illustrated in Figure 4. In all the control experiments, the condensational heating peaks much lower ($\sim$900 hPa) than the re-evaporative cooling (600 to 700 hPa). Conceptually, the former generates positive buoyancy for lifting an air parcel. As the parcel rises, it entrains drier/colder environmental air and detrains cloud condensate, which then re-evaporates into the environment. Similar to condensation, the total heating is bottom-heavy, but with a distinct local minimum owing to re-evaporation.

234 Both condensation and cloud liquid re-evaporation are stronger in the perturbed

235 energy balance, with a secondary weakening of rain re-evaporation. Although the com-

236 bined effect is integrated vertically to near zero, it is characteristic of a dipole (cooling

237 above warming) structure as $\delta C$ is more bottom-heavy than $\delta EC$. The positive buoy-

238 ancy resulting from this pattern is consistent with the enhancement of $M_c$ (Figure 1f).

239 Given that the initial perturbation is applied through modifying cloud liquid, one may

240 speculate that it is the stronger re-evaporative cooling that destabilizes the lower tro-

241 posphere and promotes stronger convection (condensation). This explains why conden-

242 sation and cloud liquid re-evaporation vary in the same direction, and constitutes a dy-

243 namical mechanism of the microphysically induced convective adjustment.

## 4  Discussion and Conclusions

245 As an anchor point of this work, the re-evaporation efficiency ($\alpha$) is an emergent

246 property of the RCE simulations, and is closely associated with tropospheric relative hu-

247 midity and convective mass fluxes across a wide range of model configurations and per-

248 turbations. It has been shown that the increase in $\alpha$ due to higher $N_d$ can be linked to

249 stronger condensation by invoking the simple theory ($\delta\alpha \simeq (1-\alpha)\delta C/C$), which can

250 also be used to explain, at least qualitatively, the large difference in $\alpha$ among the four

251 control experiments (from 0.368 in RE to 0.664 in FU). Although it is clear from our re-

252 sults that the treatment of cloud microphysics has a direct bearing on $\alpha$, convective dy-

253 namics also plays an essential role, as evidenced by the destabilizing effect of cloud liq-

254 uid re-evaporation. In light of its importance for understanding tropospheric relative hu-

255 midity (Romps, 2014), convectively coupled tropical variations and general circulation

256 (Emanuel, 2019) and climate sensitivity (Zhao et al., 2016), the potential use of $\alpha$ for

257 comparing a variety of model simulations (limited-domain and global CRMs, and coarse-

258 resolution global climate models or GCMs) and observations (Noone, 2012) should be

259 explored.

260 A contemporaneous study by Abbott and Cronin (2020) offers a way to examine

261 the robustness of our results to the choice of model configurations and experimental de-

262 signs. Both studies find that an increase in $N_d$ gives rise to higher mid-tropospheric rel-

263 ative humidity and convective invigoration in RCE simulations, even in the absence of

264 ice microphysics. While this work centers over convective invigoration (manifested as stronger

convective mass flux) in RCE, Abbott and Cronin (2020) focuses on changes in high-percentile vertical velocities under the assumption of weak temperature gradient balance.

Ice microphysical processes are often thought to play a key role in enhancing convection under polluted conditions. In the setting of RCE with prescribed radiative cooling, we demonstrate that an increase in cloud droplet number concentration can cause stronger convective mass flux even in the absence of ice microphysics. Subsequent sensitivity tests of liquid microphysical processes indicate that cloud liquid re-evaporation plays a more important role in driving the convective invigoration than rain re-evaporation. A process-level analysis reveals that higher cloud droplet number concentration slows down the conversion of cloud liquid to rain, giving rise to an increase in cloud liquid re-evaporation and a decrease in rain re-evaporation, with the former outweighing the latter. The net increase in the total re-evaporation is balanced by stronger condensation. The dipole pattern of re-evaporative cooling above condensational heating is consistent with the enhancement of convective mass flux.

## Acknowledgments

## References

Abbott, T. H., & Cronin, T. W. (2020). A humidity-entrainment mechanism for microphysical invigoration of convection. *arXiv*.

Albrecht, B. A. (1989, Sep 15). Aerosols, cloud microphysics, and fractional cloudiness. *Science*, *245*(4923), 1227.

Andreae, M. O., Rosenfeld, D., Artaxo, P., Costa, A. A., Frank, G. P., Longo, K. M., & Silva-Dias, M. A. F. (2004). Smoking rain clouds over the Amazon. *Science*, *303*(5662), 1337–1342.

Chua, X. R., Ming, Y., & Jeevanjee, N.   (2019).   Investigating the fast response of precipitation intensity and boundary layer temperature to atmospheric heating using a cloud-resolving model.   *Geophysical Research Letters*, *46*(15), 9183-9192.   Retrieved from https://agupubs.onlinelibrary.wiley.com/doi/abs/10.1029/2019GL082408   doi: 10.1029/2019GL082408

Emanuel, K.   (2019).   Inferences from simple models of slow, convectively coupled processes. *Journal of the Atmospheric Sciences*(2019).   doi: 10.1175/JAS-D-18-0090.1

Fan, J., Rosenfeld, D., Yang, Y., Zhao, C., Leung, L. R., & Li, Z.   (2015).   Substantial contribution of anthropogenic air pollution to catastrophic floods in Southwest China. *Geophysical Research Letters*, *42*(14), 6066–6075.

Fan, J., Rosenfeld, D., Zhang, Y., Giangrande, S. E., Li, Z., Machado, L. A., . . . others   (2018).   Substantial convection and precipitation enhancements by ultrafine aerosol particles. *Science*, *359*(6374), 411–418.

Fan, J., Yuan, T., Comstock, J. M., Ghan, S., Khain, A., Leung, L. R., . . . Ovchinnikov, M.   (2009).   Dominant role by vertical wind shear in regulating aerosol effects on deep convective clouds.   *Journal of Geophysical Research: Atmospheres*, *114*(D22).

Heikenfeld, M., White, B., Labbouz, L., & Stier, P.   (2019).   Aerosol effects on deep convection: the propagation of aerosol perturbations through convective cloud microphysics. *Atmospheric Chemistry and Physics*, *19*(4), 2601–2627.

Hong, S.-Y., Noh, Y., & Dudhia, J.  (2006).  A new vertical diffusion package with an explicit treatment of entrainment processes. *Monthly Weather Review*, *134*(9), 2318–2341.

Khairoutdinov, M., & Kogan, Y.   (2000).   A new cloud physics parameterization in a large-eddy simulation model of marine stratocumulus.   *Monthly Weather Review*, *128*(1), 229–243.

Langhans, W., Yeo, K., & Romps, D. M.   (2015).   Lagrangian investigation of the precipitation efficiency of convective clouds.   *Journal of the Atmospheric Sciences*, *72*(3), 1045–1062.

Lutsko, N. J., & Cronin, T. W.  (2018).  Increase in precipitation efficiency with surface warming in radiative-convective equilibrium. *Journal of Advances in Modeling Earth Systems*.

328  Morrison, H.  (2012).  On the robustness of aerosol effects on an idealized supercell
329       storm simulated with a cloud system-resolving model.  *Atmospheric Chemistry*
330       *and Physics*, *12*(16), 7689–7705.

331  Morrison, H., Thompson, G., & Tatarskii, V.  (2009).  Impact of cloud microphysics
332       on the development of trailing stratiform precipitation in a simulated squall
333       line: Comparison of one-and two-moment schemes.  *Monthly Weather Review*,
334       *137*(3), 991–1007.

335  Noone, D.     (2012).     Pairing measurements of the water vapor isotope ratio with
336       humidity to deduce atmospheric moistening and dehydration in the tropical
337       midtroposphere. *Journal of Climate*, *25*(13), 4476–4494.

338  Romps, D. M. (2014). An analytical model for tropical relative humidity. *Journal of*
339       *Climate*, *27*(19), 7432–7449.

340  Rosenfeld, D., Lohmann, U., Raga, G. B., O'Dowd, C. D., Kulmala, M., Fuzzi, S.,
341       . . . Andreae, M. O. (2008). Flood or drought: how do aerosols affect precipita-
342       tion? *Science*, *321*(5894), 1309–1313.

343  Stevens, B., & Feingold, G. (2009). Untangling aerosol effects on clouds and precipi-
344       tation in a buffered system. *Nature*, *461*(7264), 607.

345  Storer, R. L., & van den Heever, S. C.   (2013).   Microphysical processes evident in
346       aerosol forcing of tropical deep convective clouds.    *Journal of the Atmospheric*
347       *Sciences*, *70*(2), 430–446.

348  Tao, W.-K., Chen, J.-P., Li, Z., Wang, C., & Zhang, C.   (2012).   Impact of aerosols
349       on convective clouds and precipitation. *Reviews of Geophysics*, *50*(2).

350  Tao, W.-K., Li, X., Khain, A., Matsui, T., Lang, S., & Simpson, J.    (2007).    Role
351       of atmospheric aerosol concentration on deep convective precipitation: Cloud-
352       resolving model simulations.    *Journal of Geophysical Research: Atmospheres*,
353       *112*(D24).

354  Twomey, S. (1974). Pollution and the planetary albedo. *Atmospheric Environment*,
355       *8*(12), 1251–1256.

356  van den Heever, S. C., Stephens, G. L., & Wood, N. B.    (2011).    Aerosol indirect
357       effects on tropical convection characteristics under conditions of radiative–
358       convective equilibrium. *Journal of the Atmospheric Sciences*, *68*(4), 699–718.

359  Wang, S., & Sobel, A. H. (2011). Response of convection to relative sea surface tem-
360       perature: Cloud-resolving simulations in two and three dimensions.   *Journal of*

361    *Geophysical Research: Atmospheres*, *116*(D11).

362    Williams, E., Rosenfeld, D., Madden, N., Gerlach, J., Gears, N., Atkinson, L., ...
363        others    (2002).    Contrasting convective regimes over the Amazon: Implica-
364        tions for cloud electrification.    *Journal of Geophysical Research: Atmospheres*,
365        *107*(D20), LBA–50.

366    Zhao, M., Golaz, J.-C., Held, I. M., Ramaswamy, V., Lin, S.-J., Ming, Y., ... others
367        (2016).    Uncertainty in model climate sensitivity traced to representations of
368        cumulus precipitation microphysics. *Journal of Climate*, *29*(2), 543–560.

**Table 1.**    Domain-average column-integrated condensation ($C$), total re-evaporation ($E$), rain re-evaporation ($ER$), cloud condensate re-evaporation ($EC$), accretion ($AR$), precipitation ($P$) in different cases. Also included is the re-evaporation efficiency ($\alpha$). The differences between the control and perturbation simulations (the latter minus the former) are in parentheses. Except for $\alpha$ (unitless), all values are in mm day$^{-1}$. The last column ($\widetilde{\delta\alpha}$) is based on a simple theory for $\delta\alpha$, i.e. $(1-\alpha)\delta C/C$.

|      | $C$         | $E$       | $ER$       | $EC$      | $AR$       | $P$       | $\alpha$        | $\widetilde{\delta\alpha}$ |
|------|-------------|-----------|------------|-----------|------------|-----------|-----------------|------------|
| FU   | 13.7 (0.9)  | 9.1 (0.8) | 3.7 (-0.7) | 5.4 (1.5) | 8.2 (-0.6) | 4.5 (0.1) | 0.664 (0.014)   | 0.022      |
| LI   | 10.2 (1.1)  | 5.8 (1.0) | 2.7 (-0.6) | 3.1 (1.6) | 7.1 (-0.5) | 4.5 (0.1) | 0.569(0.033)    | 0.046      |
| RE   | 7.6 (1.3)   | 2.8 (1.3) | 0.5 (-0.2) | 2.3 (1.4) | 5.2 (-0.1) | 4.7 (0.1) | 0.368 (0.092)   | 0.108      |
| CE   | 9.1 (0.5)   | 4.7 (0.5) | 2.7 (-0.6) | 2.0 (1.1) | 7.1 (-0.6) | 4.4 (0.0) | 0.505 (0.026)   | 0.027      |
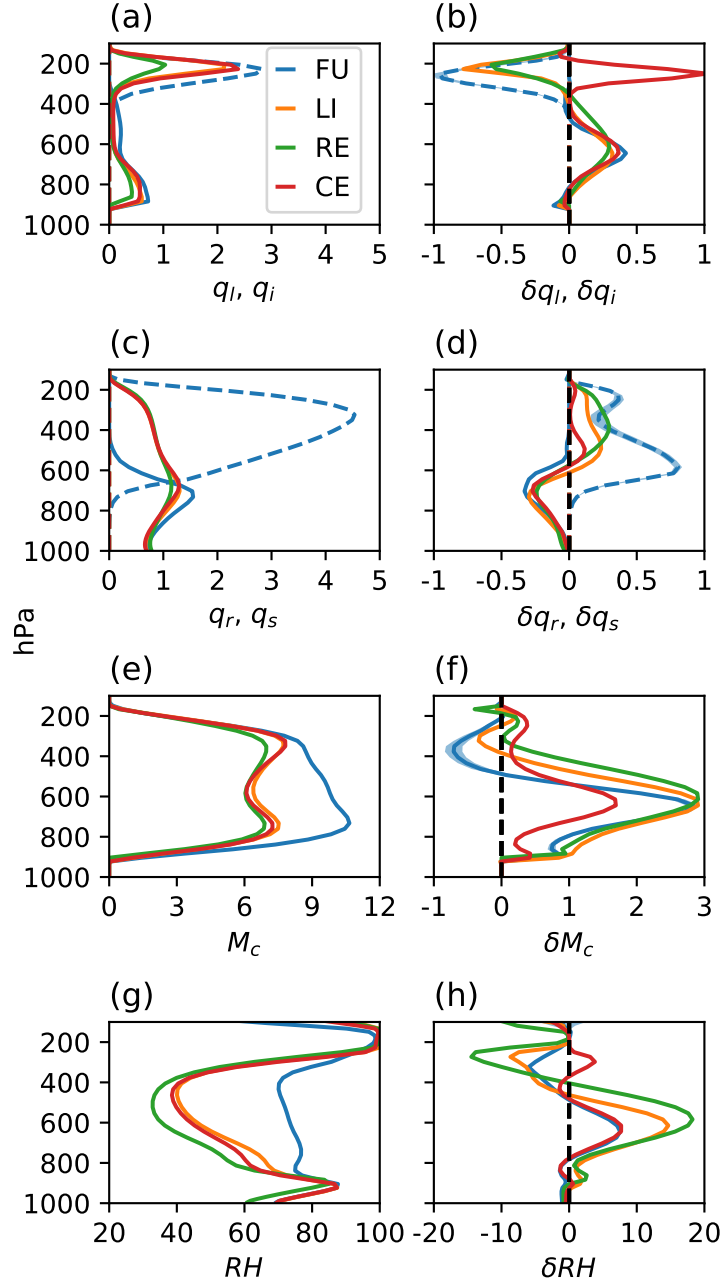
**Figure 1.** Vertical profiles of the domain-average (a)-(b) cloud liquid (solid, $q_l$, $10^{-5}$ kg$^{-1}$ kg$^{-1}$) or ice (dashed, $q_i$, $10^{-5}$ kg$^{-1}$ kg$^{-1}$) mixing ratio, (c)-(d) rain (solid, $q_r$, $10^{-5}$ kg$^{-1}$ kg$^{-1}$) or snow (dashed, $q_s$, $10^{-5}$ kg$^{-1}$ kg$^{-1}$) mixing ratio, (e)-(f) convective mass flux ($M_c$, g m$^{-2}$ s$^{-1}$) and (g)-(h) relative humidity ($RH$, %). The control experiments are in the left column, and the difference between the control and perturbation experiments are in the right column. The shading denotes the noise levels in FU. Note that cloud ice and snow are present only in FU and FU*
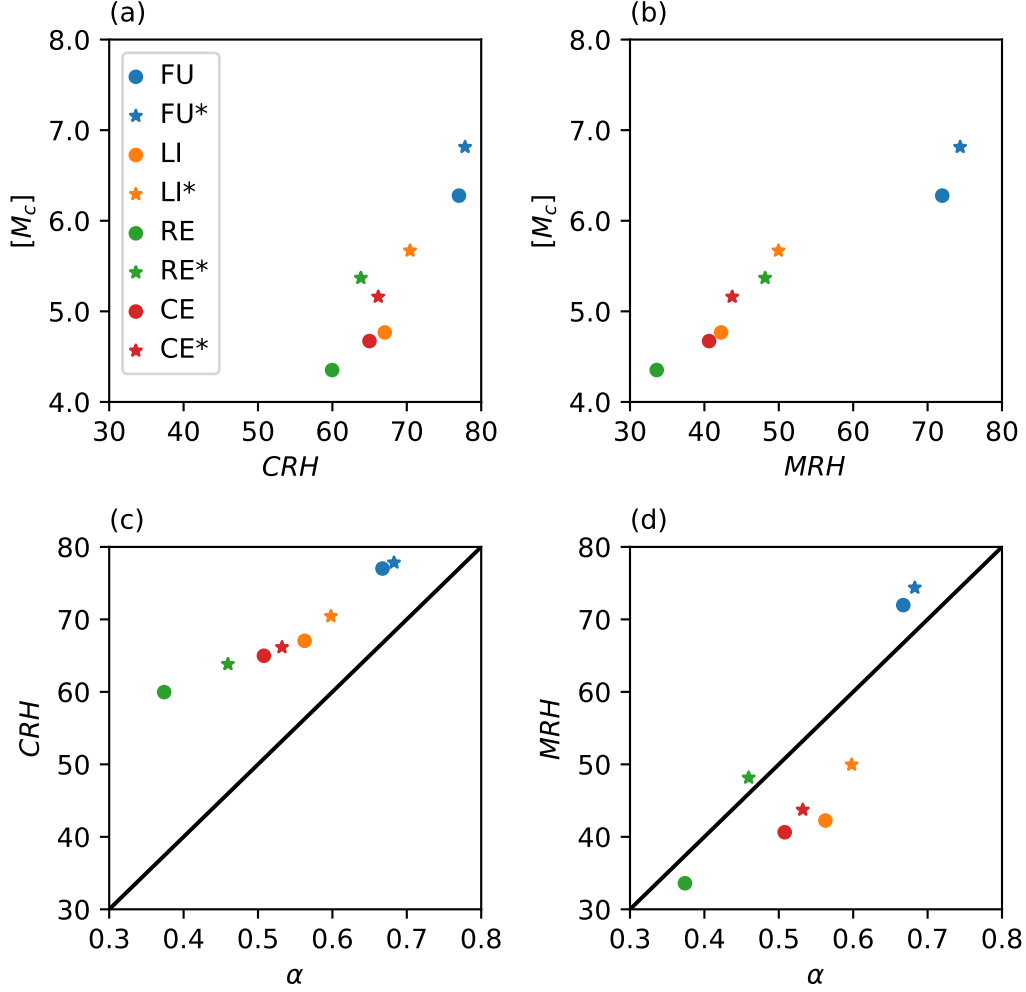
**Figure 2.** Scatter plots of (a) vertically averaged convective mass flux ($[M_c]$, g m$^{-2}$ s$^{-1}$) versus column relative humidity ($CRH$,%), (b) $[M_c]$ versus mid-tropospheric (400 to 600 hPa) relative humidity ($MRH$, %), (c) $CRH$ versus the re-evaporation ratio ($\alpha$, unitless), and (d) $MRH$ versus $\alpha$ in all experiments.
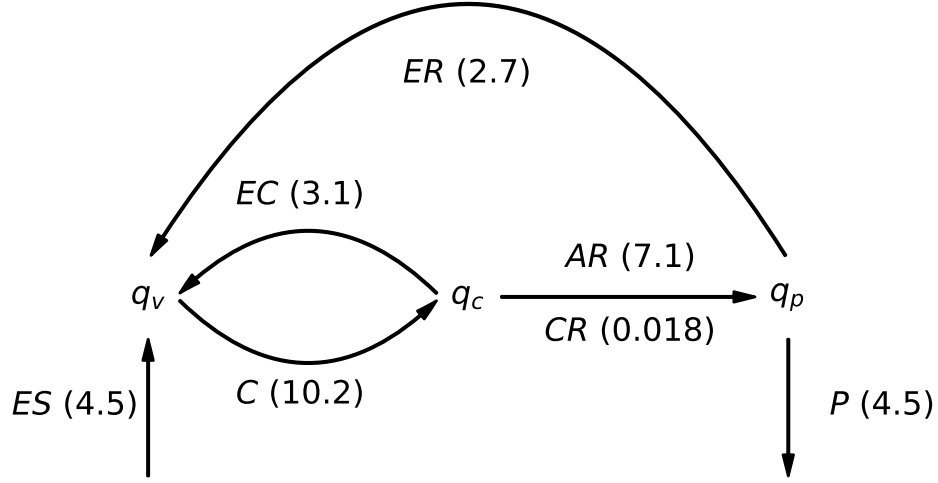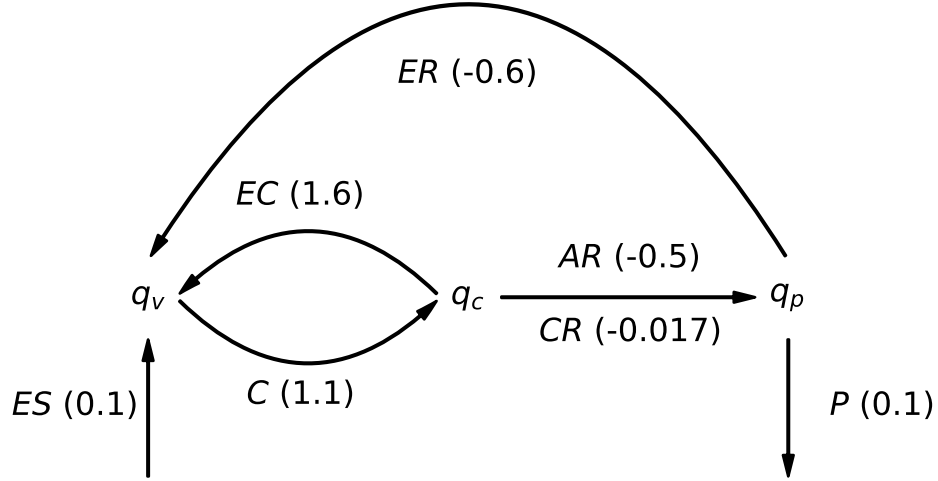
**Figure 3.** Domain-average column-integrated rates (mm day$^{-1}$) of microphysical processes involving water vapor ($q_v$), cloud condensates ($q_c$) and hydrometeors ($q_p$) [condensation of cloud condensates ($C$), re-evaporation of cloud condensates ($EC$), conversion of cloud water to rain by autoconversion ($CR$) and accretion ($AR$) and re-evaporation of rain ($ER$)], as well as surface evaporation ($ES$) and precipitation ($P$). (a) is the LI control experiment, and (b) the difference between LI and LI*. The corresponding values for all configurations are listed in Table 1.
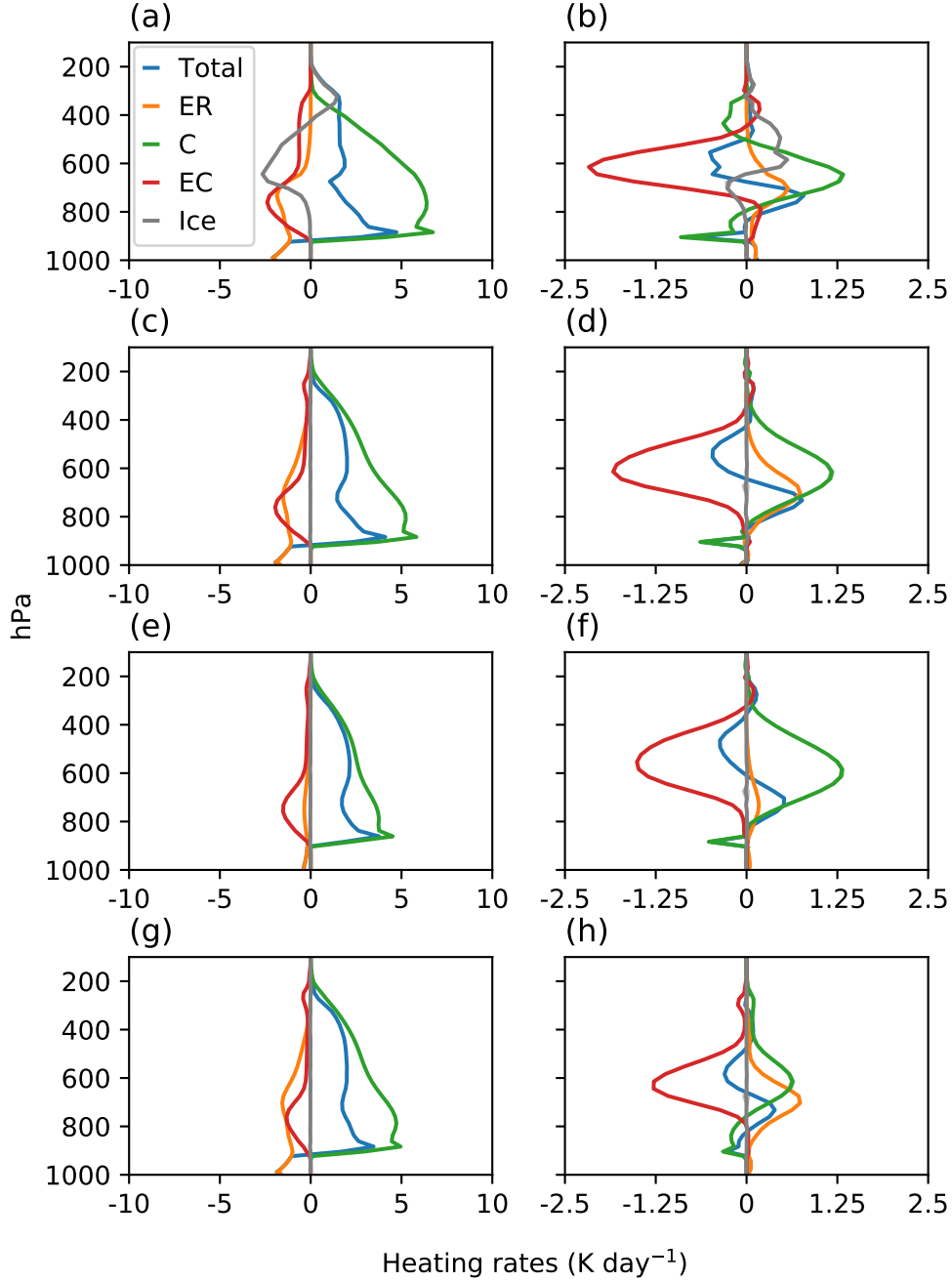
**Figure 4.** Vertical profiles of the domain-average heating rates (K day$^{-1}$) due to condensation ($C$), rain re-evaporation ($ER$), cloud condensate re-evaporation ($EC$), ice microphysics (Ice) and the total (Total). The control experiments are in the left column, and the difference between the control and perturbation experiments are in the right column. (a)-(b) are for FU, (c)-(d) for LI, (e)-(f) for RE, and (g)-(h) for CE.
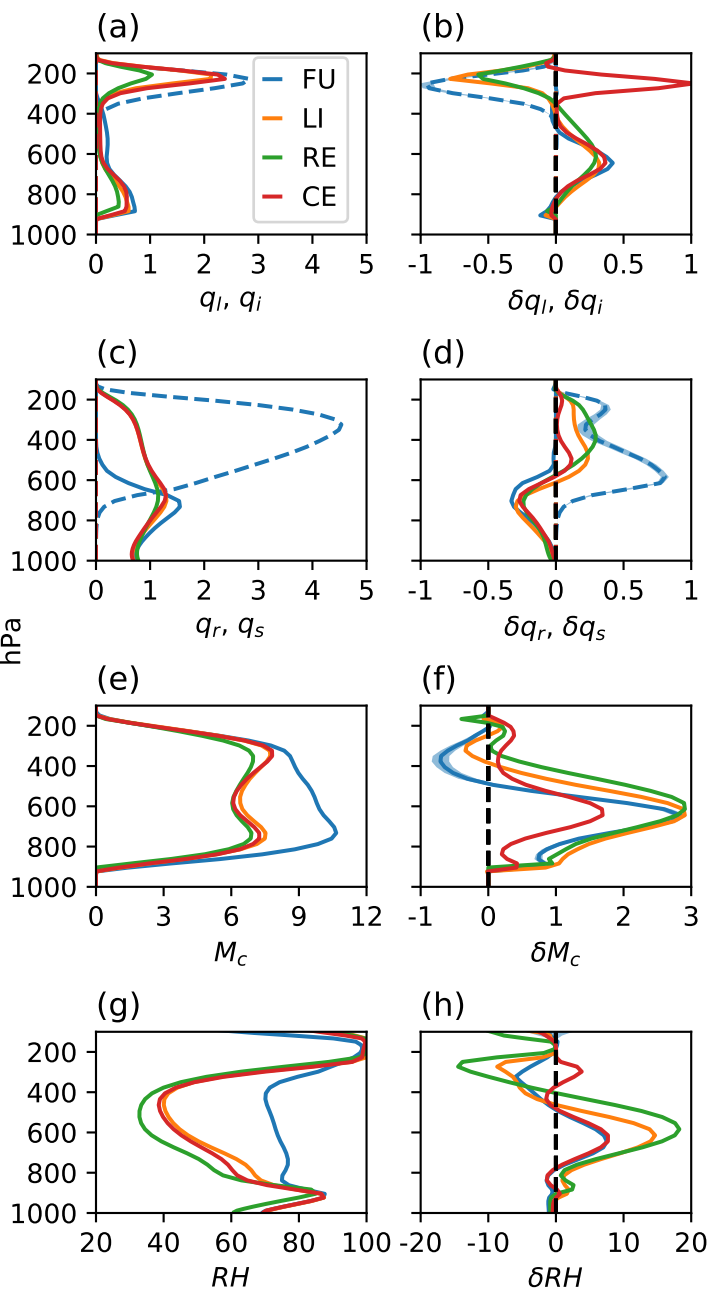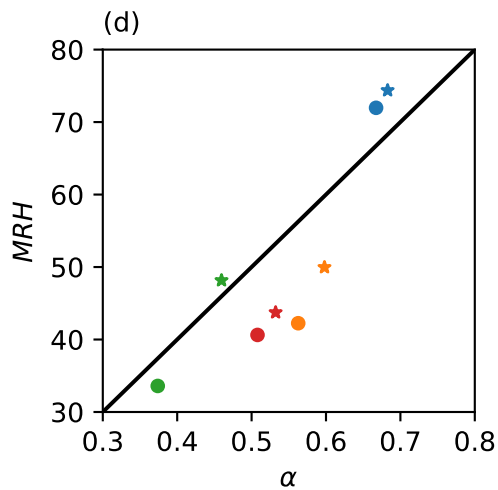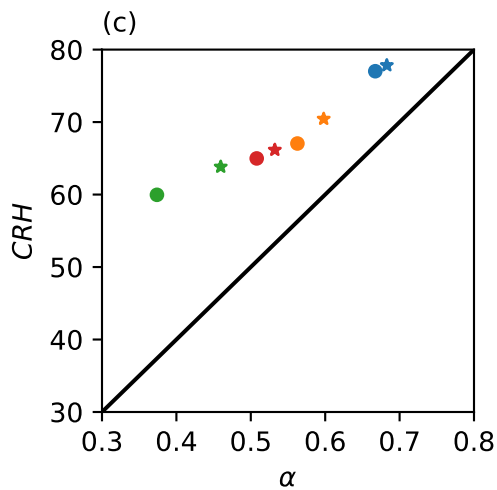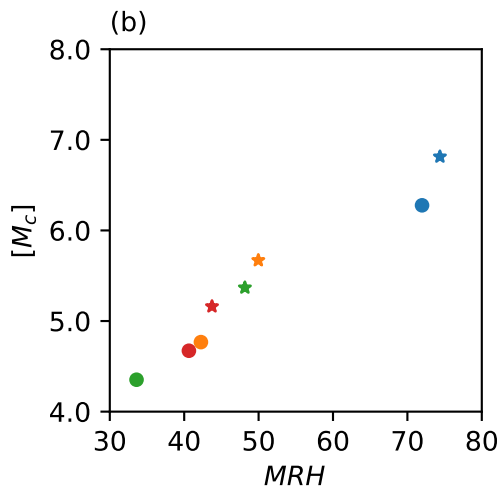
**Figure1.**

**Figure2.**

**Figure3.**

(a)

ER (2.7)

EC (3.1)

$q_v$     $q_c$     AR (7.1)     $q_p$

CR (0.018)

ES (4.5)     C (10.2)     P (4.5)

(b)

ER (-0.6)

EC (1.6)

$q_v$     $q_c$     AR (-0.5)     $q_p$

CR (-0.017)

ES (0.1)     C (1.1)     P (0.1)

**Figure5.**

Heating rates (K day$^{-1}$)
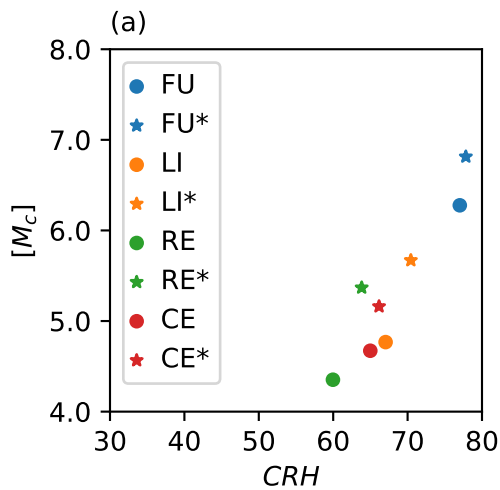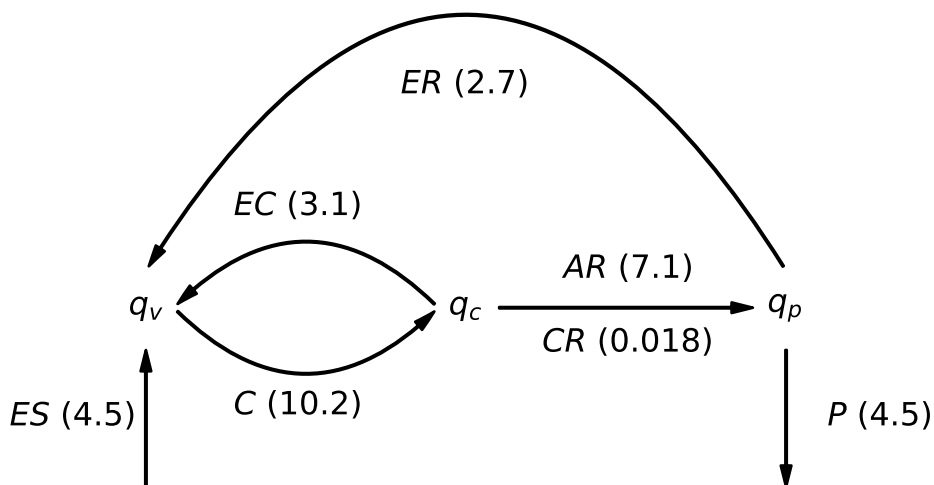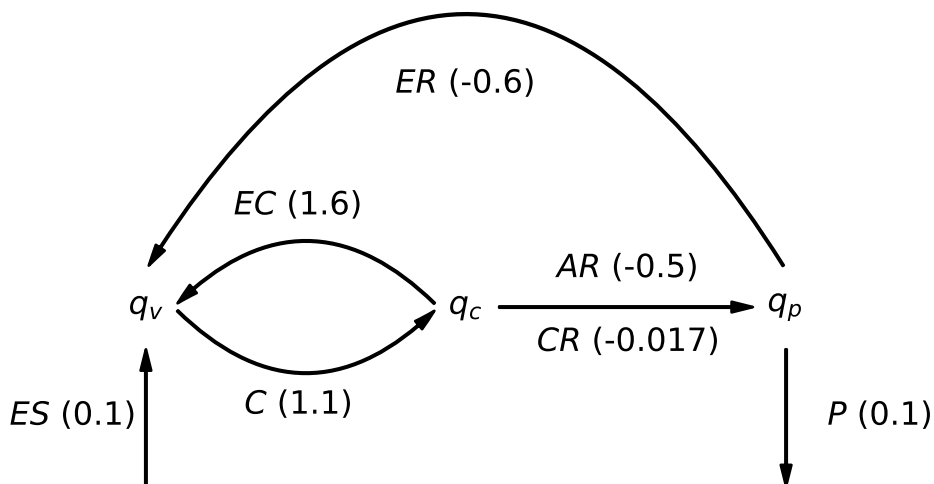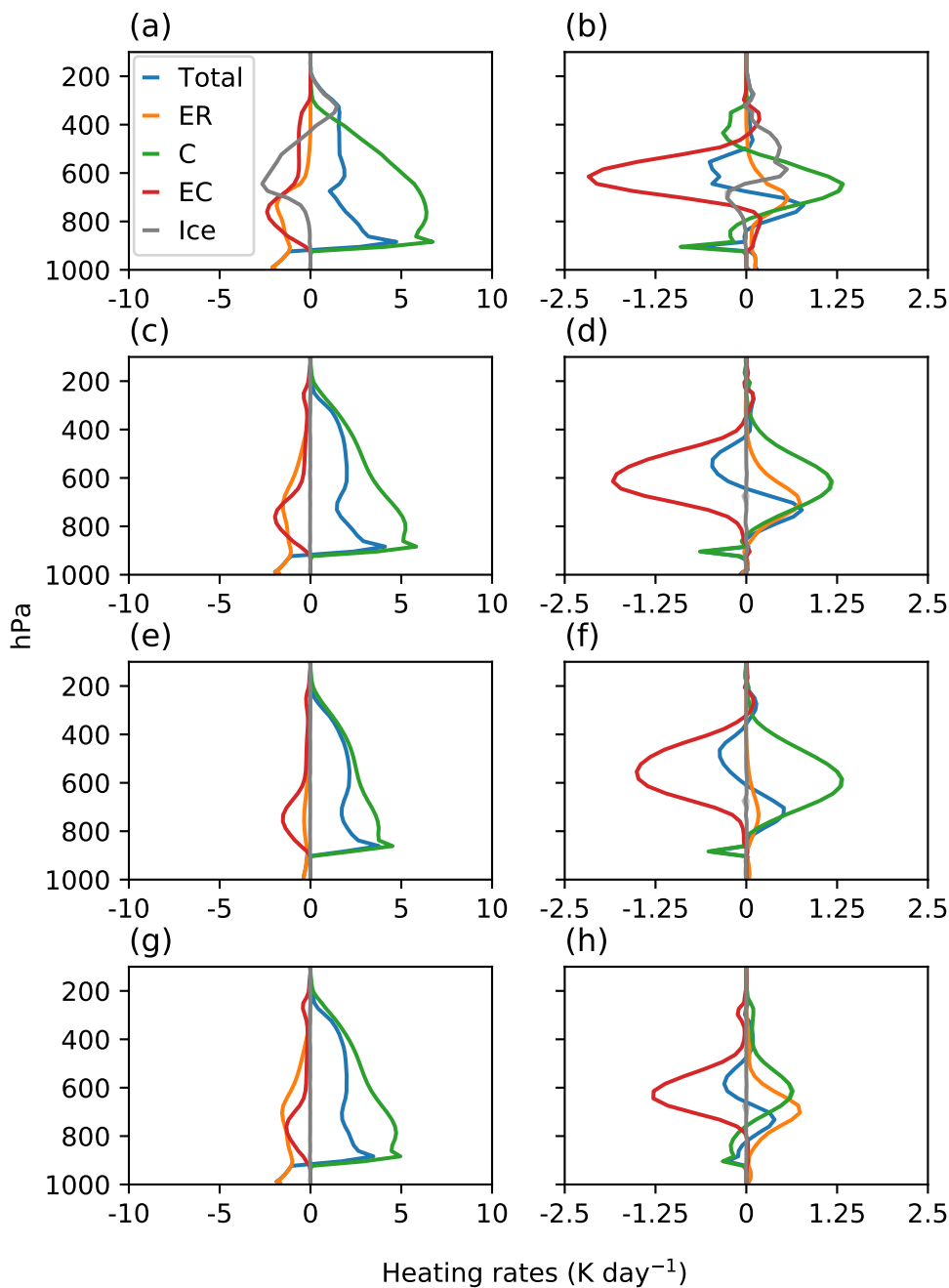
# Supporting Information for"Convective invigoration traced to warm-rain microphysics"

Xin Rong Chua[1] [*], Yi Ming[1,2]

[1]Program in Atmospheric and Oceanic Sciences, Princeton University, Princeton, New Jersey, USA

[2]Geophysical Fluid Dynamics Laboratory, Princeton, New Jersey, USA

## Contents of this file

1. Table S1

[*]Current affiliation: Centre for Climate

Research Singapore, Singapore

January 15, 2020, 2:19am

**Table S1.** Additional ice processes included in the calculation of the terms in Table 1 in the

FULL cases.

| Included in | Process |
|---|---|
| $AR$ | Cloud droplet accretion by snow |
| | Cloud droplet collection by graupel |
| | Cloud droplet collection by snow to graupel |
| | Accretion of cloud ice by snow |
| | Autoconversion of cloud ice by snow |
| | Ice-rain collection |
| | Ice-rain collision (added to snow) |
| | Conversion of large ice to snow |
| | Ice multiplication (rain and snow) |
| | Ice multiplication (rain and graupel) |
| $EC$ | Sublimation of cloud ice |
| $C$ | Deposition of cloud ice |
| | Primary ice nucleation |
| $ER$ | Sublimation of graupel |
| | Sublimation of snow |
| | Evaporation of graupel |
| | Evaporation of snow |
| | Deposition of graupel |
| | Deposition of snow |